

OPTIMIZATION AND CHARACTERIZATION OF A MICROSCALE THERMAL FIELD-FLOW FRACTIONATION SYSTEM

Himanshu J. Sant¹, Bruce K. Gale²

State of Utah Center of Excellence for Biomedical Microfluidics,
Departments of Bioengineering, and Mechanical Engineering, University of Utah,
50 S. Central Campus Drive, Rm. 2110, Salt Lake City UT 84112, USA

Corresponding author: ¹himanshu.sant@utah.edu, Phone: +1 801-581-6549
²gale@eng.utah.edu, Phone: +1 801-792-7074, URL: www.mems.utah.edu

Abstract

A thorough investigation of the design considerations for microscale thermal field-flow fractionation and characterization of a 25 μm thin microscale thermal field-flow fractionation system is reported. A 4-50 times volume reduction from mesoscale and macroscale systems warrants customized design and operational conditions for microscale separation systems. Theoretical calculations are done to illustrate the importance of the increased dispersion due to extra-column tubing, off-chip detection and sample injection volume with reduced channel dimensions. An optimized microscale thermal field-flow fractionation (ThFFF) channel is fabricated using rapid and cost effective manufacturing and assembly processes. Specifically, improvements in material selection and arrangement are implemented to achieve higher particle retentions. The new instrument arrangement includes high conductivity silicon as the cold wall and a thin polymer layer with low thermal conductivity as the hot wall which results in high temperature gradients ($\sim 10^6$ $^{\circ}\text{C}/\text{m}$) across the microchannel and subsequently high retention. Single particle retention separations are carried out with polystyrene nanoparticle samples in an aqueous carrier to characterize the device and demonstrate the improvements.

Key Words: Separation, Field-Flow Fractionation, Chromatography, Microfluidics, Nanoparticles, Retention

1. Introduction

In the last few years, microscale field-flow fractionation (FFF) based techniques have generated substantial interest from researchers, as indicated by an increase in the number of publications in this field [1,2,3]. A wide range of FFF subtypes with different geometric dimensions that range from microscale to mesoscale have been reported [4-8]. Typically, microscale systems have channel heights of the order of 10-50 μm and channel volumes less than 10 μL .

With miniaturization, both operating conditions and system integration approaches should be carefully chosen in order to obtain high resolution separations [1]. Microscale FFF systems require careful packaging and interconnections with the minimum possible pre-column and post-column volumes, including minimal detector volumes with on-chip detection as the preferred option [1,4,9]. In addition, operating conditions such as carrier flowrate should be optimized so as not to increase band dispersion and early peaks due to inadequate sample relaxation. Thus, a number of design and operational issues need to be considered while optimizing a microscale field-flow fractionation system, which is the focus of this paper (exemplified by characterization of thermal FFF).

Lately, great progress in the development of mesoscale thermal systems has been reported by Janca *et al* [10]. They reported typical channel thicknesses of 100-250 μm and utilization of the same fabrication methods utilized since the 1960's to fabricate ThFFF macroscale systems [11]. By using a 23 μm thin and 96 mm long channel with a 1 μL sample injected, using an injection loop with no results, the authors concluded that smaller microscale systems will only produce poor retention and resolution [12]. The main problem with such an arrangement is that the sample volume is more than 12% of the total channel volume and with an injection time of 1 minute, the sample occupies a large volume in the channel with the potential for considerable band broadening, even if the sample is fully relaxed. With relatively high flowrates (6 ml/hr) for a typical microsystem and use of off-chip detectors, the result is poor resolution, entirely due to improper operating conditions. In comparison to macroscale systems, the sample volume and sample concentration in a microsystem present a bigger challenge for proper operation. In FFF, a relaxed sample is concentrated as a very thin layer near the accumulation wall. Even a low concentration sample stream becomes focused to the

point that it becomes a compact layer. Then the sample stream washes over the compact sample leading to early elution. If the sample volume is high, a significant portion of the sample will be excluded from the compact layer typical in FFF and increased secondary effects arise, such as particle-particle and wall repulsion effects, causing increased peak-broadening, reduced retention, and more importantly, poor repeatability [13]. The high sample volume may have resulted in the poor resolution for 23 μm microscale ThFFF [12]. In microsystems, this effect seems to be more pronounced when compared to macroscale systems due to the much smaller particle cloud to channel thickness ratios [9]. Our experience with FFF microsystems has shown that 0.1 - 0.2 μL injection volumes provide reasonable results [1,9]. This paper reports the operating conditions for ThFFF system that results in powerful retention of nanoparticles.

Another important design aspect related to miniaturization is minimization of the instrumental plate height [14]. In particular, post-column tubing and detector volumes need to be as small as possible, as was shown by the difference in obtainable resolution by an electrical FFF microsystem employing off-chip and on-chip detectors [4, 9]. Similar results should be expected for other FFF systems employing other types of fields such as thermal FFF. The variation of the plate height contribution with scaling to indicate important design and operating considerations for microscale FFF systems is discussed here.

Recently Janca group has reported excellent results using a Thermal FFF system at mesoscale that was build using methods reported in 1960s by Giddings group [15,16,17]. Our paper reports a microscale thermal FFF system with an improved design [18] when compared to systems used in earlier communications [6,12, 19]. This microscale thermal FFF system was fabricated without the use of extensive microfabrication techniques [2].

Thermal FFF utilizes a temperature gradient perpendicular to the flow direction to induce retention (Figure 1) [1]. A major consideration when designing a microscale ThFFF system is the choice of channel wall materials and their geometric arrangement due to the high heat fluxes involved with $\mu\text{-ThFFF}$. The high heat fluxes inherently require the system to be provided with an efficient heat exchanger on the cold wall side to maintain the required temperature gradient ($\sim 10^6\text{C/m}$) across the thin microchannel.

Otherwise, the result will be a low temperature drop and poor retention [6]. Ideally, the walls of the channel should be made of a material with high thermal conductivity for efficient heat transfer and uniform heat distribution, but a good insulation layer is required to prevent heat loss from the hot wall. To address this design challenge, the thermal microsystem reported here uses a hot wall made of thin plastic (high heat capacity) and silicon with high thermal conductivity. It should be noted that a system with copper walls will require much smaller heater power and coolant flow rates to achieve the required temperature drop as compared to a plastic hot wall with the same geometrical dimensions. Reduced hot wall thickness reduces the power required to as low as 10 to 15 W, thus justifying the design change for a given temperature drop.

In this paper, we report a μ -thermal FFF system fabricated using rapid prototyping techniques [2]. A knife plotter was used to pattern microchannels from a tape with adhesive applied on both sides and bonded to the plastic and silicon substrate to create a composite μ -thermal system. The plastic substrate was machined to create corrugation with only a thin layer of material remaining, into which a thin film heater is placed. The power required to heat the hot side of the channel and the time to reach a steady state temperature are reduced due to a substantial reduction in the thermal mass of the substrate, which results in a reduced load on the heat exchanger that is maintaining the cold wall temperature at a constant value. The newly designed microsystem was employed to characterize the particle retention in an aqueous environment using a thermal field.

2. Theory

The goal of any separation system optimization effort is to maximize the separation efficiency (reduce plate height) and resolution or fractionating power. The total plate height can be depicted as the summation of several contributing factors such as non-equilibrium effects, H_n , instrumental effects, H_i , polydispersity, H_p and the contribution due to diffusion, H_D [20] as given by

$$H = H_n + H_i + H_p + H_D. \quad (1)$$

The non-equilibrium part of the plate height is given by

$$H_n = \frac{\chi(\lambda)w^2\langle v \rangle}{D}. \quad (2)$$

where, w is the channel height, $\langle v \rangle$ is the average velocity and D is the particle diffusion coefficient. The details on the function $\chi(\lambda)$ and other plate height related factors are detailed elsewhere [14,20].

Other plate heights that need to be considered during the optimization efforts of microscale systems are related to the sample volume, sample relaxation and extra-column tubing and detector volumes [20].

The plate height contribution due to the sample volume injection is given by

$$H_s = \frac{v_{inj}^2}{12(b/w)^2 w^2 L} \quad (3)$$

where, v_{inj} is the volume of the sample injected, and b and L are the channel width and length respectively [20].

The plate height contribution, H_r , due to the sample relaxation is given by

$$H_r = \frac{17}{140} \frac{h_0^2}{L}, \quad (4)$$

where, h_0 is the span of the fully relaxed sample along the channel length and can be related to the retention parameter, λ and flow velocity by

$$h_0 = \frac{w \langle v \rangle}{\lambda D} \quad [23] \quad (5)$$

The main band broadening related contributions due to the off-chip detector are related to the volume of the detector, V_c' , [20]

$$H = \frac{1}{L} \left(\frac{V_c'}{bw} \right)^2 \quad (6)$$

and length of the extra-column tubing, L_t ,

$$y = \frac{L_t \dot{V} L \pi r_t^4}{48 D V r^2 H}, \quad (7)$$

where, V_r' is the retention volume, y is the plate height factor, \dot{V} is the volumetric flowrate and r_t is the radius of the extra-column tubing [20].

While the plate height contributions represented through equations 2 to 4 have been reported for FFF and general chromatography, this paper will closely review the effects of scaling on these factors with respect to optimization efforts for the microsystem.

The retention parameter for thermal-FFF is given by

$$\lambda = \frac{D}{D_T \Delta T}, \quad (8)$$

where, D_T is the thermal diffusion coefficient and ΔT is the temperature drop across the channel height.

3. Experimental

3.1. Band Broadening Calculations

The channel geometries used for the scaling analysis related to band broadening were channel (1) 25 μm height, 2 mm width and 9 cm length, (2) 100 μm height, 2 mm width and 9 cm length and (3) 200 μm height, 2 cm width and 40 cm length. The average velocity used was 2.78 mm/s. The molecular diffusion coefficient used is $1 \times 10^{-8} \text{ cm}^2/\text{s}$.

3.2. Materials

3.2.1. Samples

Polystyrene nanoparticles of the diameters 91 nm, 130 (carboxylated) and 209 nm were purchased from Bangs Laboratories, Fishers, IN). These nanoparticles were diluted with DI water to 1% concentration by weight from the original sample to avoid detector saturation and overloading of the separation channel. Sample injection volume for all experiments was 0.2 μL .

3.2.2. Carrier

Filtered DI water (Model D 8611, Barnstead International, IA) of 18.2 $\text{M}\Omega\cdot\text{cm}$ was used as the carrier for all the experiments. A 3 CC gastight glass syringe (Model 1005, Hamilton CO., NV) was used to deliver fresh carrier fluid for each run.

3.3. Methods

3.3.1. Instrument Fabrication and Assembly.

The instrument fabrication, assembly and packaging are similar to the methods published elsewhere [19]. In earlier designs, a microbaricated ThFFF system, with boron-doped silicon as hot wall and glass as the cold wall, generated a poor temperature drop across the channel thickness [6]. The basic design was modified from those proposed in these early reports by changing the hot and cold wall materials. Silicon with high thermal conductivity is used as the cold wall and polished glass/HDPE with high heat capacity as the hot wall [18,19]. A heat exchanger is provided to the cold wall to

remove the excessive heat flux associated with the microsystems. The high thermal conductivity of silicon assists in rapid heat removal. Thin hot wall with high heat capacity material keeps the hot wall temperature steady, while still allowing for heat conduction across the microchannel. Figure 2 shows a schematic of the various components of the micro thermal field-flow fractionation (μ -ThFFF) system prior to assembly.

A syringe pump (Model 220, KD Scientific Inc., MA) was used to deliver a constant flow of carrier fluid to the microsystem. The sample particles were injected using a microliter syringe (Model 701, Hamilton CO., NV) through a T-injector to the input port of the microchannel. The other end of the T-injector is connected to the syringe pump that allows the flow of the carrier fluid in to the ThFFF channel that is routed to an off chip UV absorbance detector (Model 520, ESA Inc, MA). The connecting tube is 4 cm long with 0.0762 cm inside-diameter. The elution /retention time of the sample was measured by the first moment of the elution peak recorded electronically using data acquisition hardware (DAQ card, model PC 6023 E, National Instruments, Inc. TX) and interface software (Lab VIEW 6.1, National Instruments, Inc. TX). A DC power supply Tektronix PS 280 was connected to the ThFFF instrument to power the thin film heater.

3.3.2. Plate Height Measurements

The properties of fractograms were used to measure the plate height variation with temperature drop. From plate theory, the plate height, H can be calculated from the experimental data from the half peak width and elution peak volume as described elsewhere [1,21].

3.3.3. Retention Experiments.

The ThFFF system was characterized by conducting retention experiments using polystyrene nanoparticles (diameters ranging from 91 nm to 209 nm). The temperature drop for the thermal field ranged from 20°C to 45°C. The flowrate range for these experiments was 0.5 to 1.5 ml/hr. The sample injection volume was 0.2 μ L. The retention time is converted to retention volume by multiplying with the carrier flowrate after subtracting the time taken by the sample to reach from the microsystem through post-column tubing to the detector flowcell.

All the experiments were geared towards obtaining data on retention time as this information can be converted directly to retention ratio. This retention ratio value was used to gauge the performance of the μ -ThFFF system by comparing the experimental results with the theoretical predictions.

The main objectives of these experiments were to (i) determine the optimal protocols and operational conditions and (ii) study the effect of important parameters that govern retention in a ThFFF system. The most important parameter of interest is temperature gradient. Other factors to be considered are flowrate, carrier composition, and sample size. The main retention related experiments involved (i) the use of μ -ThFFF system to produce retention of the sample particles using thermal field and (ii) variation of the operational parameters such as temperature, flowrate and particle size.

4. Results and Discussion

4.1. Band-Broadening Calculations

4.1.1. Effect of Finite Injected Sample Volume

There are primarily two ways that sample is introduced into an FFF channel: (i) an impulse injection using a microliter syringe and (ii) slow sample injection with an injection valve at very low flowrates compared to the carrier flowrate during the separation.

Equation 3 is applicable to the cases where a finite volume of sample is injected into the FFF channel under no-field conditions. It is clear that the use of a 1 μ L sample leads to very high plate height contribution when compared to the non-equilibrium plate height contribution for 25 μ m channels (Figure 3). Plate height calculations with a 0.1 μ L sample injection show a close to 100 times decrease in the sample volume induced plate height over the entire range of the retention parameter (λ). Use of a microliter syringe for sample injection causes only slight deviations in results when compared to instances where stop-flow sample relaxation is used. It should be noted that the sample volume is an important factor that needs to be as small as possible especially for microsystems. The sample volume is also related to sample overloading in other FFF studies that clearly show reduced retention and increased band broadening for high sample volumes [22].

4.1.2. Effect of Detector and Post-Column Volumes

Equation 6 can be used to estimate the optimum detector flowcell volume. As long as the flowcell volume is much smaller than the volume obtained from equation 6, the effect of the off-chip detector should be negligible.

The flowcell volume calculated from equation 6 for channels 1, 2 and 3 (see experimental section for the geometrical dimensions) are $\sim 0.5 \mu\text{L}$, $20 \mu\text{L}$, and $750 \mu\text{L}$ respectively. It should be noted that there is a 20% change in this calculated volume when the retention ratio changes from 0.3 to 0.05 with the non-equilibrium plate height being calculated from equation 2. Hence, the use of a $1.2 \mu\text{L}$ flowcell with a $25 \mu\text{m}$ thick channel should increase the band broadening which should otherwise be negligible for $100 \mu\text{m}$ and $200 \mu\text{m}$ thick channels. For this reason, the analysis of the resolution results should be done carefully, otherwise poor resolution may be attributed to the small channel heights instead of the nonidealities originating from the inadequate design and operating conditions as reported elsewhere [12].

Apart from the contribution due to the detector volume, the presence of post-column tubing connecting the microchannel and flowcell can also contribute significantly to the overall band broadening and should be taken into account in resolution estimates.

It can clearly be seen that even a short connecting tube section joining the microsystem to an off-chip detector causes a substantial increase in band broadening as indicated by the % standard deviation of the peak at the end of the connecting tube in Figure 4. Figure 4 also shows the negligible effect of the presence of the connecting tube on overall band broadening in the case of $100 \mu\text{m}$ and $200 \mu\text{m}$ systems that allow the use of a longer tube and multiple off-chip detectors in series.

4.2. *Effect of Temperature Drop*

Selection of proper materials for the hot and cold wall allowed us to get a very high temperature drop (as high as $40 \text{ }^\circ\text{C}$) as compared to the poor temperature drop of only 5°C reported elsewhere [6]. Figure 5 shows the fractograms obtained of 130 nm (carboxylated) polystyrene particles at different temperature drops across the channel thickness of the $\mu\text{-ThFFF}$ system. This plot clearly shows the ability to tune the retention time for the single diameter particles by changing the field. Some of the observations that can be made from the traces in Figure 5 are (i) the 15 s relaxation time has very little effect on the baseline of the detector response as the particles pass through the detector

flowcell, (ii) the considerable peak broadening originates due to the off-chip detector with a 1.2 μL flowcell and its connecting tube.

Another important observation related to the experiments in thermal FFF is related to the sample recovery. We noted that the amplitude of the detector response over time decreased with the prolonged use of the microchannel and sample adsorption to the accumulation wall may be causing this effect. Use of a thin layer of titanium on the channel walls and a small amount of detergent such as FL-70 (even less than 1%) in the carrier solution reduces the sample adsorption to the wall.

4.3. Plate Height Measurements

Plate heights can be used to measure the undesirable band broadening in FFF and should be minimized to obtain high resolution separations. Plate height measurements done for the fractograms shown in Figure 5 indicate the trend expected according to FFF theory as shown in Figure 6. At low temperature drop or low effective field, the retained sample is less compact than for higher temperature drops and diffuses away from the accumulation wall in the channel height direction. This enlarged particle cloud experiences higher velocity zones of the parabolic velocity profile in the $\mu\text{-ThFFF}$ channel resulting in more axial dispersion and more particle band broadening. At high retention, the sample particles are forced to assume more a compact form that experiences only a small change in velocities and remains as a tighter band in the axial direction also. Thus, with an increase in the applied field, the band broadening reduces and a higher resolution can be obtained along with longer retentions.

The retention data shown in Figure 7 follows a normal-mode relationship for thermal field-flow fractionation for a variety of flowrates for the 130 nm (carboxylated) diameter particles. The retention in FFF does not vary with flowrate according to the retention theory (equation 8). It should be noted that the unexplained retention data reported in Figure 5 of the reference [12] clearly departs from this theoretical observation. In addition, the numerical analysis results do not show any change in the temperature gradient across the channel height with flow velocity (assuming high heat transfer), which otherwise would have resulted in the retention change with flow velocity as reported by Janca *et al* [12].

With an increase in temperature drop across the microchannel, the retention increases. Excellent retention of 130 nm particles can be obtained with an adequate temperature drop (40 °C). The design improvements and proper material choice with an efficient heat exchanger maintaining a low cold wall temperature allows for much higher retention when compared to previous microscale thermal FFF reports [6]. These retention values are comparable to macroscale thermal FFF systems which are much bulkier and consume considerably higher power with larger analysis times. It should be noted that a better temperature control should result in better temperature drop-retention correlation. The current thermocouple probes are placed on the sides of the hot wall and the back side of the cold wall. A better arrangement would be an on-chip thermocouple adjacent to the microchannel on either wall that can be connected to a feedback temperature controller.

Observation of the results also provided some helpful guides for performing experiments. For example, the mean temperature of the stream eluting from the microchannel should not be very high, as this results in unwanted spikes and deterioration of the peak shape.

4.4. Comparison to Theory

Equation 8 is used to calculate the retention parameter and subsequently theoretical retention ratios that are shown as a solid line in Figure 7. The molecular and thermal diffusion coefficients used for these calculations are $2.8 \times 10^{-8} \text{ m}^2/\text{s}$ and $3.6 \times 10^{-8} \text{ m}^2/\text{s K}$, respectively [23]. The theoretical model matches better with the experimental data at high retention or low retention ratios as shown in Figure 7. One of the reasons for the deviations from the theory is that we have not measured the molecular or thermal diffusion coefficients for the particles; instead we have used literature values for the theoretical calculations. As the normal diffusion coefficient or the nature of the velocity profile in ThFFF are temperature dependent and proper corrections to that effect should be made in the future models to get a better fit for the experimental data. In addition at low field strengths, sample is lost with the void peak as shown in Figure 5, which could be another contributing factor to deviation from theory. Sample relaxation with an initial area or period of high field strength should reduce such sample loss.

4.5. *Effect of Sample Size*

The retention parameter in thermal-field-flow fractionation is given by equation 8. The Soret coefficient, the ratio of thermal diffusion to diffusion, and Brownian diffusion coefficient, are a complex function of the important FFF operational parameters such as temperature, carrier properties, and the sample size and the samples interaction with the carrier. The thermal diffusion coefficient in particular is known to have a clear dependence on particle size [24,25]. With a molecular diffusion coefficient dependence on the particle size, the size selectivity of the thermal FFF instrument will be more than unity, indicating the thermal-diffusion coefficient variation with the particle diameter or molecular weights. The microscale thermal FFF presented here has shown a size selectivity greater than unity as shown in Figure 8, suggesting that microscale ThFFF would be appropriate for polymer size determination.

5. **Conclusion**

Theoretical and experimental results show how a thin μ -ThFFF with proper design and optimization of the operational parameters can produce a high temperature drop across the microchannel and much improved retention compared to the previous reports. The improved design of the microsystem has resulted in very good retention using an aqueous carrier (e.g. retention ratio of ~ 0.008 can be obtained for 130 nm (carboxylated) diameter particles). The optimization efforts show the importance of the sample volume and extra-column volumes with the channel height (or channel volume) scaling, which is applicable to all microscale FFF systems. The experimental results closely follow theory, but a tighter control on the operating condition will be required in future work to employ this microsystem towards the analytical applications.

Figure Captions

Figure 1. Diagram of a FFF system operation showing the input and output ports, application of the thermal field, the parabolic flow profile, and relative channel dimensions. The thermal FFF system employs a temperature gradient to induce the separation with a fluid channel encompassed by hot and cold walls.

Figure 2. Assembly chart for the μ -ThFFF device. The thermocouple array and heater consist of a thin film encapsulated in polyimide, and the microchannel is made from a 25 μm thick double-sided adhesive tape. Black circles on the sides of plastic slide indicate thermocouple holes for the thermocouple probes.

Figure 3. Plot of % contribution of the plate height due to a 1 μL sample injection (equation 3) in comparison to the plate height due to the non-equilibrium component (equation 2). The three simulated traces are for channels with 25 μm , 100 μm and 200 μm thicknesses. The geometrical dimensions of each of these channels with varying thicknesses are detailed in the experimental section.

Figure 4. Plot of % change of the peak due to the connecting tube (0.01 inch diameter and 5 cm length) for channels of the thickness 25 μm , 100 μm and 200 μm (see experimental section for the geometrical dimensions for each channel).

Figure 5. Plot of fractograms showing the effect of temperature drop on the elution of 130 nm (carboxylated) particles from a μ -ThFFF channel. The temperature drop between hot and cold wall is in the range of 15°C to 40°C and each fractogram is identified with the associated temperature drop by an arrow in the Figure 5. The flowrate for these experimental runs was 0.8 ml/hr. The data shown here is without subtraction of the time taken by the sample to reach the detector through the post-column tubing.

Figure 6. Plot of plate heights measured for the fractograms shown in Figure 5.

Figure 7. Plot showing the effect of temperature drop on the retention ratio of 130 nm (carboxylated) particles from μ -ThFFF. The flowrate range used for these experiments is 0.5 to 1.5 ml/hr.

Figure 8. Plots of retention dependence on particle diameter.

Figure 1.

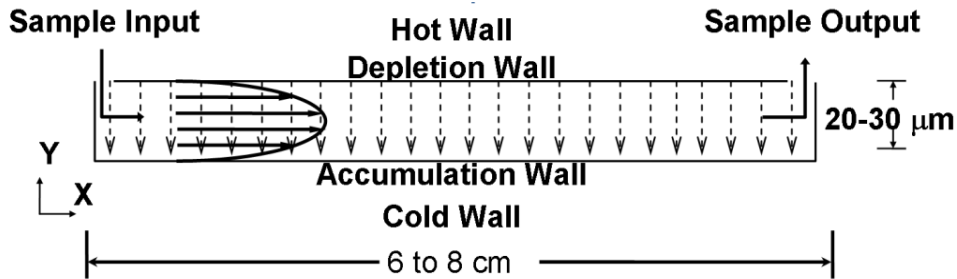


Figure 2.

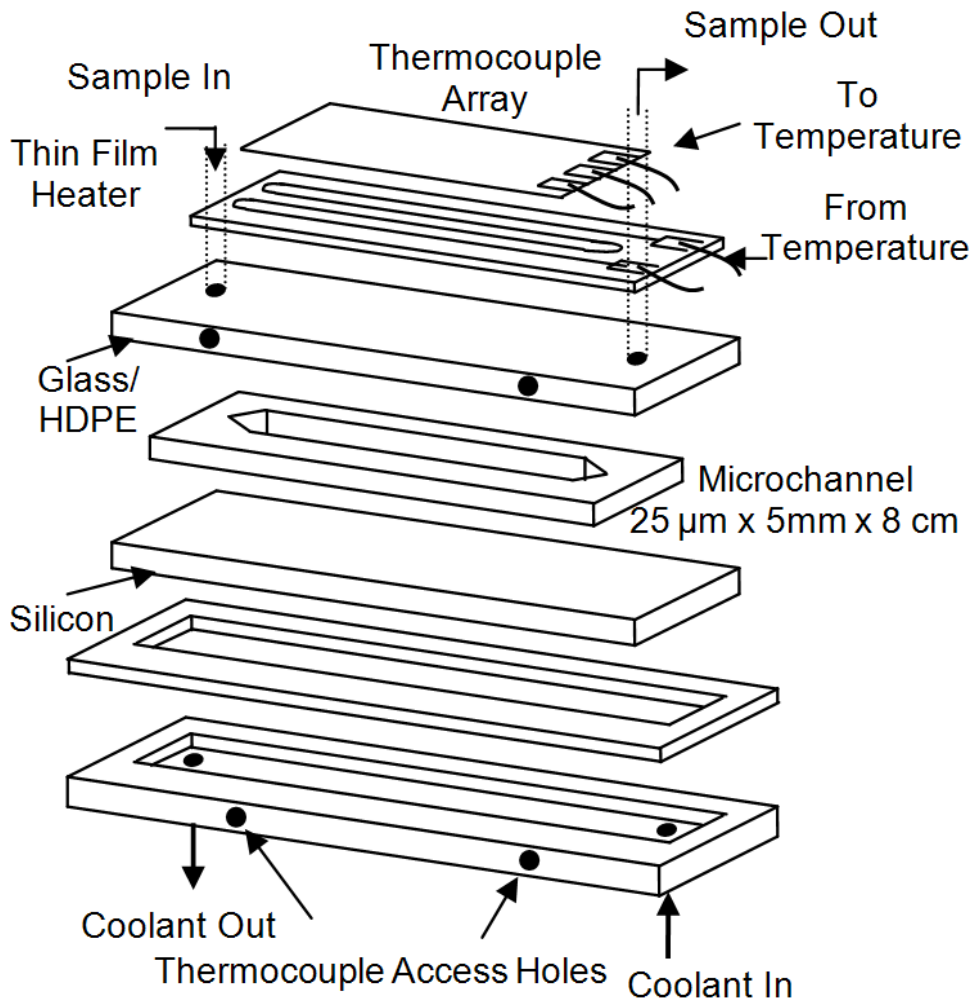


Figure 3.

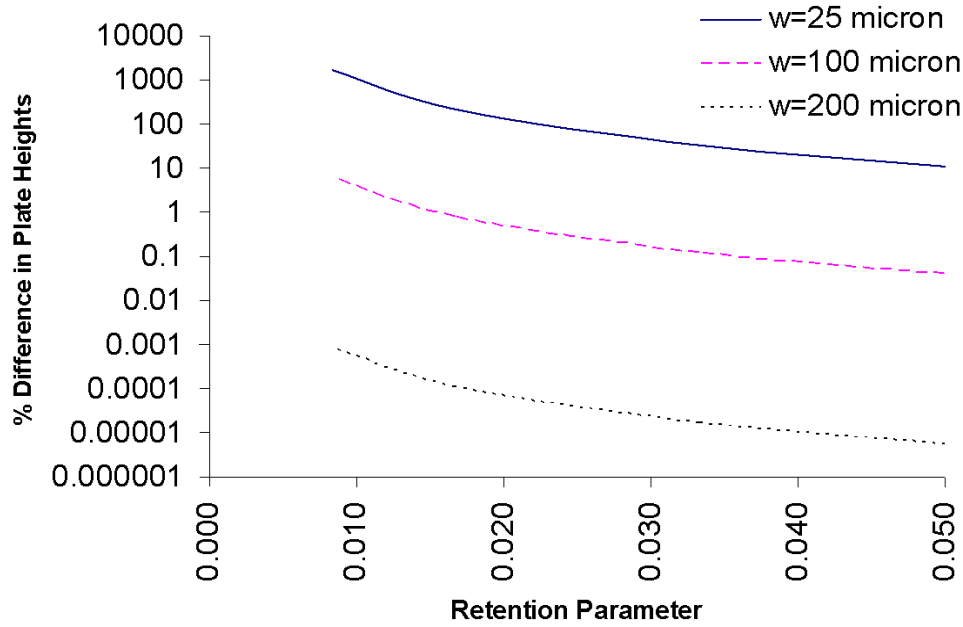


Figure 4.

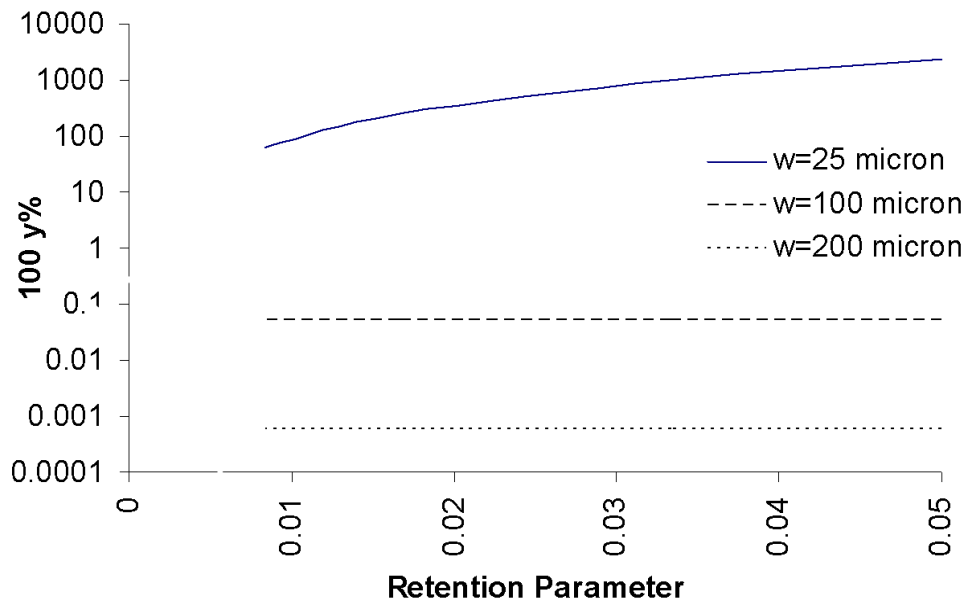


Figure 5.

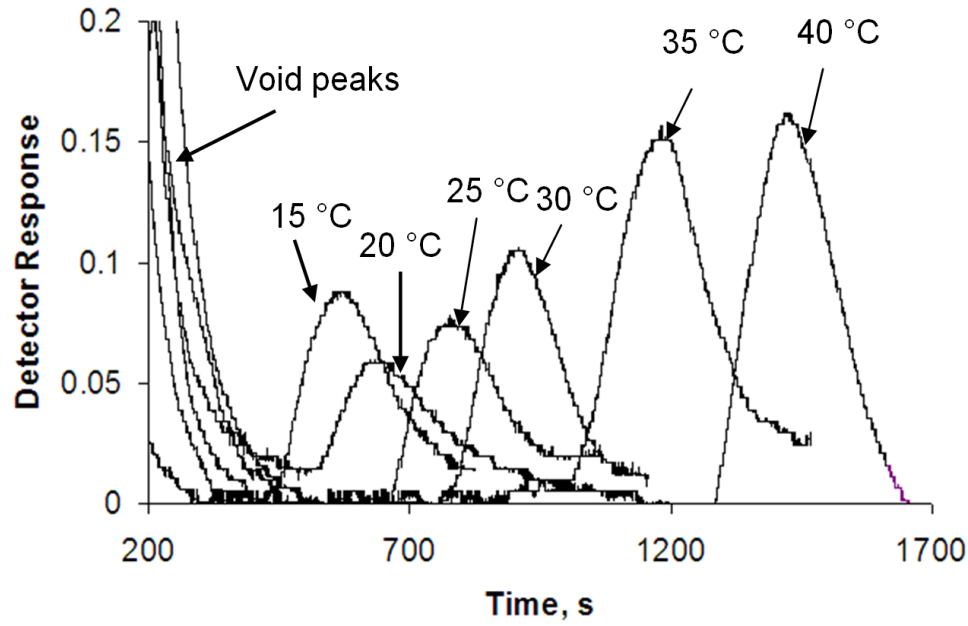


Figure 6.

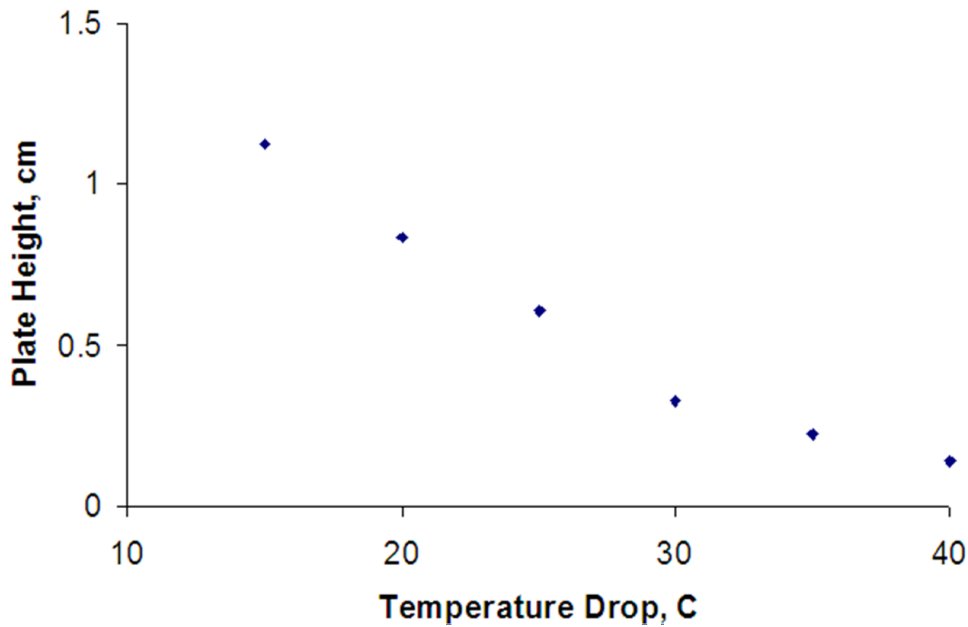


Figure 7.

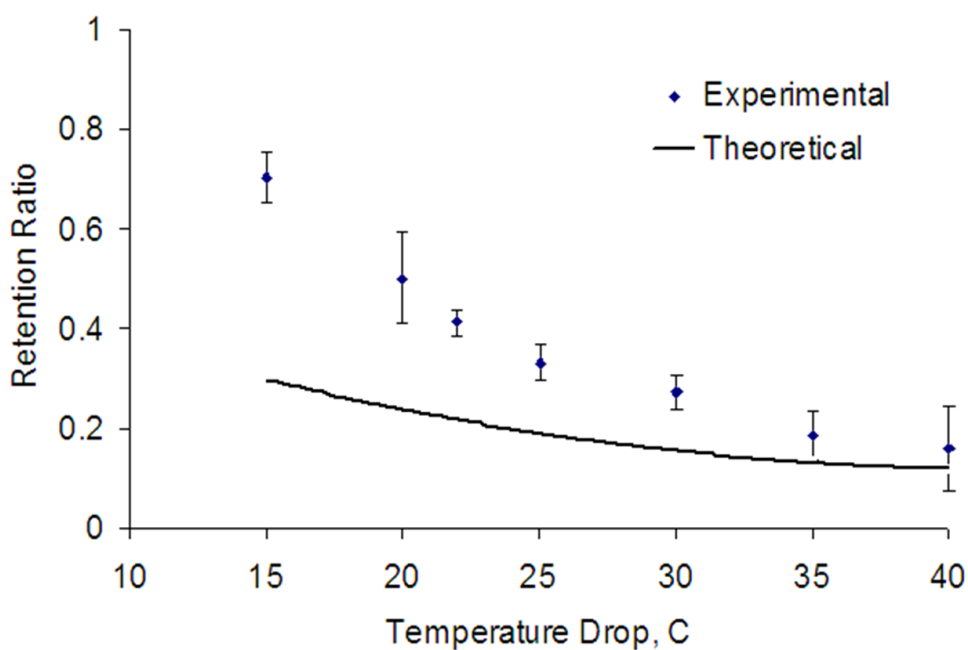
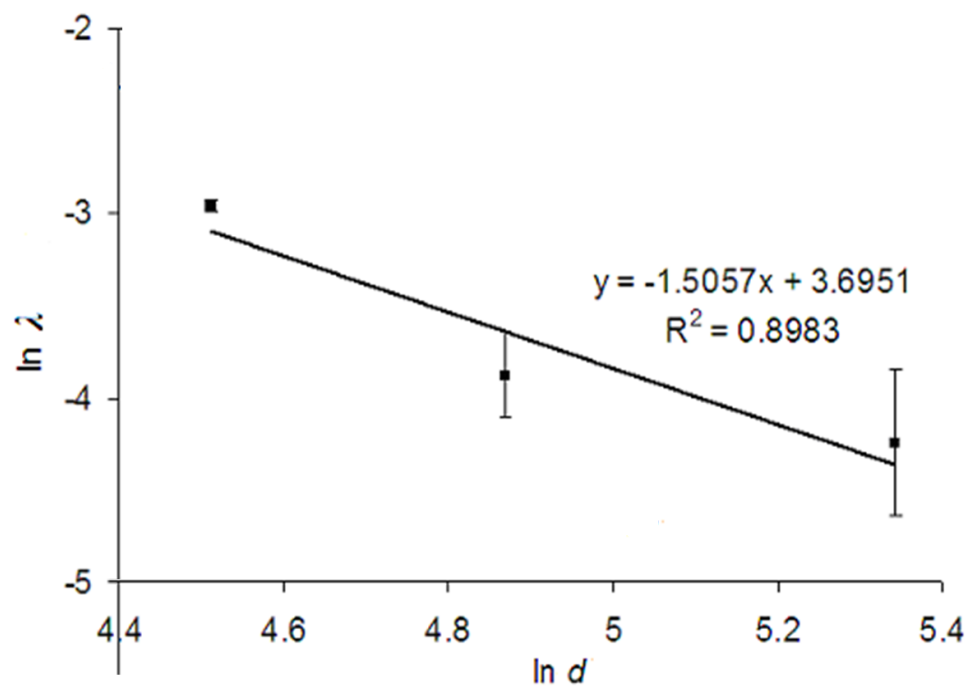


Figure 8.





References

- [1] H. J. Sant, B. K. Gale, *Microscale Field-flow fractionation: Theory and Practice*, in: S. Hardt S, F. Schönfeld (Eds.), *Microfluidic Technologies for Miniaturized Analysis Systems*, Springer-Verlag, Berlin, Germany, 2007, pp. 471-522.
- [2] Himanshu J. Sant and Bruce K. Gale, "Flexible fabrication, packaging, and detection approach for microscale chromatography systems," *Sens. Act. B*, Vol. 141, No. 1, pp. 316-321, 2009
- [3] B. Weiss, W. Hilber, P. Gittler, B. Jakoby, Particle separation in alternating-current electro-osmotic micropumps using field-flow fractionation, *Microfluid. Nanofluid.* 7 (2009) 191-203.
- [4] B. K. Gale, K. D. Caldwell, A. B. Frazier, A Micromachined Electrical Field-Flow Fractionation System, *IEEE Trans. Biomed. Eng.* 45 (1998) 1459-1469.
- [5] A. I. K. Lao, D. Trau, I. Hsing, Miniaturized Flow Fractionation Device Assisted by a Pulsed Electric Field for Nanoparticle Separation, *Anal. Chem.* 74 (2002) 5364-5369.
- [6] T. E. Edwards, B. K. Gale, A. B. Frazier, A Microfabricated Thermal Field Flow Fractionation System, *Anal. Chem.* 74 (2002) 1211-1216.
- [7] J. Yang, Y. Huang, X.-B. Wang, F. Becker, R. Gascoyne, Cell Separation on Microfabricated Electrodes Using Dielectrophoretic/Gravitational Field-Flow Fractionation, *Anal. Chem.* 71 (1999) 911-918.
- [8] D. Kang, M. Moon, Miniaturization of Frit Inlet Asymmetrical Flow Field-Flow Fractionation, *Anal. Chem.* 76 (2004) 3851-3855.
- [9] B. K. Gale, K. D. Caldwell, A. B. Frazier AB, Geometric Scaling Effects in Electrical Field- Flow Fractionation. 2. Experimental Verification, *Anal. Chem.* 74 (2002) 1024-1030
- [10] J. Janča, Polarization, steric, and focusing micro-thermal field-flow fractionation principles, theory, instrumentation, and applications in polymers and particles analysis, *Anal. Chim. Acta* 540 (2005) 187-196.
- [11] J. C. Giddings, New separation concept based on a coupling of concentration and flow non-uniformities, *Sep. Sci.* 1 (1966) 123-125.
- [12] J. Janča, Effect of channel width on the retention of colloidal particles in polarization, steric, and focusing micro-thermal field-flow fractionation, *J Chromatogr A* 1046 (1994) 167-173.
- [13] K. D. Caldwell, Y. S. Gao, Electrical field-flow fractionation in particle separation. 1. Monodisperse standards, *Anal. Chem.* 65 (1993) 1764-1772.
- [14] H. J. Sant, J. W. Kim, B. K. Gale, Reduction of End Effect-Induced Zone Broadening In Field Flow Fractionation Channels, *Anal. Chem.* 78 (2006) 7978-7985.
- [15] J. Janča, J. Stejskal, On the retention mechanisms and secondary effects in microthermal field-flow fractionation of particles, *J Chromatogr. A* 1216 (2009) 9071-9080.
- [16] J. Janča, V. Halabalova, J. Růžička, Role of the shape of various bacteria in their separation by Microthermal Field-Flow Fractionation, *J Chromatogr. A* 1217 (2010) 8062-8071.

- [17] G. Liu, J. C. Giddings, Separation of Particles in Nonaqueous Suspensions by Thermal-Electrical Field-Flow Fractionation, *Anal. Chem.* 63 (1991) 296-299.
- [18] H. J. Sant, B. K. Gale, A Microfabricated Thermal Electric Field-flow fractionation System, in: 5th International Conference on Miniaturized Chemical and Biochemical Analysis Systems, Monterrey, California, October 21-25, (2001) 563-564.
- [19] S. Bargiel, J. A. Dziuban, A. Górecka-Drzazga, A micromachined system for the separation of molecules using thermal field-flow fractionation method, *Sens Actuators A* 110 (2004) 328-335.
- [20] J. M. Davis, Band broadening and plate height. In *Field-Flow Fractionation Handbook*, in: M. E. Schimpf, K. D. Caldwell, J. C. Giddings J. C. Eds. Wiley-Interscience, New York, NY, 2000, pp. 49.
- [21] Himanshu J. Sant and Bruce K. Gale , Improved Models of Geometric Scaling Effects in Field Flow Fractionation, *J. Chromatogr. A*, 1104 (2006) 282-290.
- [22] J. Wijnhoven, J-P. Koorn, H. Poppe, W. T. Kok, Influence of injected mass and ionic strength on retention of water-soluble polymers and proteins in hollow-fibre flow field-flow fractionation , *J. Chromatogr. A*, 732 (1996) 307-315.
- [23] G. Liu, J. C. Giddings, Separation of particles in aqueous suspensions by thermal field-flow fractionation. Measurement of thermal diffusion coefficients, *Chromatographia*, 34 (1992) 483-492.
- [24] S. J. Jeon, M. E. Schimpf, A. Nyborg, Compositional Effects in the Retention of Colloids by Thermal Field-Flow Fractionation, *Anal. Chem.* 69 (1997) 3442-3450.
- [25] S. Duhr, D. Braun, Why molecules move along a temperature gradient, *PNAS*, 103 (2006) 19678-19682.